Bioengineered yeast-derived vacuoles with enhanced tissue-penetrating ability for targeted cancer therapy

Vipul Gujrati[a], Miriam Lee[b], Young-Joon Ko[b], Sangeun Lee[b], Daejin Kim[a], Hyungjun Kim[a], Sukmo Kang[a], Soyoung Lee[a], Jinjoo Kim[a], Hyungsu Jeon[a], Sun Chang Kim[a], Youngsoo Jun[b,1], and Sangyong Jon[a,1]

[a]KAIST Institute for the BioCentury, Department of Biological Sciences, Korea Advanced Institute of Science and Technology, 291 Daehak-ro, Yuseong-gu, Daejeon 305-701, Republic of Korea; and [b]School of Life Sciences and Silver Health Bio Research Center, Gwangju Institute of Science and Technology, Gwangju 61005, Republic of Korea

Despite the appreciable success of synthetic nanomaterials for targeted cancer therapy in preclinical studies, technical challenges involving their large-scale, cost-effective production and intrinsic toxicity associated with the materials, as well as their inability to penetrate tumor tissues deeply, limit their clinical translation. Here, we describe biologically derived nanocarriers developed from a bioengineered yeast strain that may overcome such impediments. The budding yeast *Saccharomyces cerevisiae* was genetically engineered to produce nanosized vacuoles displaying human epidermal growth factor receptor 2 (HER2)-specific affibody for active targeting. These nanosized vacuoles efficiently loaded the anticancer drug doxorubicin (Dox) and were effectively endocytosed by cultured cancer cells. Their cancer-targeting ability, along with their unique endomembrane compositions, significantly enhanced drug penetration in multicellular cultures and improved drug distribution in a tumor xenograft. Furthermore, Dox-loaded vacuoles successfully prevented tumor growth without eliciting any prolonged immune responses. The current study provides a platform technology for generating cancer-specific, tissue-penetrating, safe, and scalable biological nanoparticles for targeted cancer therapy.

affibody | bioengineered yeast | cancer therapy | drug delivery | yeast vacuoles

Recent decades have witnessed the emergence of the nanomedicine era in cancer diagnosis and therapy, made possible by the advent of new synthetic nanomaterials suitable for imaging or drug delivery (1, 2). Such nanomaterial-based drug delivery systems have shown improved therapeutic efficacy with lower unwanted adverse effects compared with conventional chemotherapy, at least in animal models (1–5). Despite the appreciable success of cancer nanomedicines in preclinical studies, only a few such agents have entered clinical trials, and fewer still have shown promising therapeutic outcomes and advanced to subsequent trial stages (6–8). Among factors likely to hamper the clinical feasibility of synthetic cancer-targeting nanomaterials are technical challenges involving their pilot scale, cost-effective production, and intrinsic cytotoxicity associated with these materials. In addition to these limitations, tumor tissues have formidable physiological barriers, such as a high interstitial pressure and densely entangled ECM. Most synthetic nanomaterials fail to penetrate tumor tissues deeply and localize only in perivascular areas, thereby limiting their therapeutic efficacy (6–8). To overcome the limitations associated with synthetic nanomedicines, researchers have recently developed biologically derived, nanosized vesicles as novel drug delivery systems (9–12). Minicells and outer membrane vesicles derived from genetically engineered bacteria and mammalian cell-derived exosomes have shown potent antitumor efficacy (10–14). Moreover, such biological vectors can be engineered to achieve cancer cell-specific delivery of diverse cargos by introducing cancer-targeting ligands onto their surfaces (10–12). However, concerns remain about the immunogenicity of bacteria-derived vehicles. For exosome-based delivery systems, large-scale, cost-effective methods for producing cancer cell-specific exosomes are currently bottlenecks for future

clinical applications. Thus, there is a need for a new class of biologically derived drug delivery systems that have an enhanced tissue-penetrating ability and cancer cell specificity, as well as low immunogenicity and facile drug loading, and that can be produced cost-effectively on a large scale.

To this end, we report here the development of a bio-inspired drug delivery system using vacuoles isolated from genetically engineered yeast cells that may fulfill these unmet needs. Budding yeast (*Saccharomyces cerevisiae*) is nonhazardous and nonpathogenic, and thus has been used in fermentation products for millennia (15). In addition, its simple genetic and biochemical manipulations, together with the fact that many yeast genes are conserved among higher eukaryotes, including humans, make it an ideal model for various biological studies (15, 16). Unlike bacteria, its lipid composition is similar to the composition of mammalian cell membranes, potentially increasing fusion efficiency with the plasma membrane or endolysosomes, and thereby facilitating the release of drugs into targeted cells or tissues (17–20). Exploiting these features, we genetically engineered *S. cerevisiae* to express human epidermal growth factor receptor 2 (HER2)-specific affibody on the vacuolar membrane, enabling the targeting of HER2 receptors that are expressed on various cancers (12, 21, 22). We further loaded the anti-HER2 affibody-expressing vacuoles (Affi$_{HER2}$Vacuole) with the chemotherapeutic drug doxorubicin (Dox), which is widely used in treating solid tumors. We then examined the anticancer effects of the drug-carrying, HER2-targeted vacuoles

Significance

Tumor tissues have formidable physiological barriers, such as a high interstitial pressure and a densely entangled ECM. Most synthetic nanomaterials used for drug delivery fail to penetrate tumor tissues deeply and localize only in perivascular areas, thereby limiting their therapeutic efficacy. This report describes bioengineered yeast-derived natural nanocarriers for cancer-specific targeting and drug delivery. Budding yeast was genetically engineered to produce large numbers of nanosized compartments—vacuoles that display cancer—targeting ligands on their surface. The nanosized vacuoles significantly enhanced drug penetration in tumor xenografts, and consequently prevented tumor growth without eliciting immune responses. This result shows that the biological nanocarriers overcome the limitations associated with synthetic cancer-targeting nanomaterials, and thus can be used to treat various cancers.

www.manaraa.com

(Affi$_{HER2}$Vacuole^{Dox}) and compared their anticancer efficacy with the anticancer efficacy of the free drug (Free^{Dox}); drug-free vacuoles (Affi$_{HER2}$Vacuole); and affibody-free, Dox-carrying vacuoles (Vacuole^{Dox}) in HER2-overexpressing, in vitro-cultured, cell-based models and an in vivo mouse xenograft model.

The proposed bioengineered yeast vacuole-based platform partly imparts limitations associated with synthetic cancer-targeting nanomaterials and provides inspiration and future directions for designing of an effective anticancer drug delivery system that could be considered in clinical applications to treat various cancers.

Results and Discussion

Preparation and Characterization of Cancer-Targeting Vacuoles. Although WT yeast cells have two to five large vacuoles that are around 1 μm in diameter, their size and number vary depending upon the cell cycle and environmental conditions, reflecting vacuole-associated fission and fusion events (17, 19, 20, 23). The processes of fission and fusion are tightly regulated by multiple factors, including Rab GTPases that mediate membrane tethering and docking, which are prerequisites for homotypic vacuole fusion (24–29). The major Rab GTPase for yeast vacuole fusion is yeast protein transport 7 (*YPT7*); thus, its deletion results in a large number of fragmented, nanosized vacuoles (25–27, 30–32). To obtain a high yield of nanosized vacuoles, we generated a yeast strain with a *YPT7* deletion (*YPT7Δ*) (Fig. 1*A* and Fig. S1*A*). Additionally, the yeast cells were genetically engineered to express the HER2-specific affibody on the vacuolar membrane for cancer targeting. Such modified *YPT7Δ* yeast cells contained a large number of fragmented vacuoles with enhanced colloidal stability. To express the Affibody$_{HER2}$ on the vacuolar membrane, we genetically fused the gene encoding myc-tagged Affibody$_{HER2}$ to the 5′ end of the *PHO8* gene, which encodes vacuolar transmembrane alkaline phosphatase. The Affibody$_{HER2}$-expressing vacuoles (Affi$_{HER2}$Vacuoles) were then purified as described in *SI Materials and Methods*, *Yeast Strains, Plasmid Construction, and Vacuole Isolation*. Specific expression of the *PHO8*-Affibody$_{HER2}$ chimeric protein in the Affi$_{HER2}$Vacuole was shown by Western blot analysis using antibodies against *PHO8* and the myc tag

(Fig. 1*B*). These Affi$_{HER2}$Vacuoles were characterized in terms of their size and morphology using electrophoretic light scattering (ELS) and transmission electron microscopy (TEM) (Fig. 1*C* and Fig. S1 *B* and *C*). These analyses of the Affi$_{HER2}$Vacuoles revealed a bilayered, circular morphology with a hydrodynamic diameter of ~200 nm. The HER2 specificity of the Affi$_{HER2}$Vacuole was verified by ELISA. The Affi$_{HER2}$Vacuole showed an ~14-fold higher affinity for HER2 compared with the controls (Fig. 1*D*). Importantly, after proteinase kinase (PK) treatment, the Affi$_{HER2}$Vacuole showed an almost complete loss of HER2 affinity, indicating that the functional form of the Affibody$_{HER2}$ was exposed on the exterior vacuole surface. Next, by confocal imaging, we showed that the Affi$_{HER2}$Vacuoles were specifically bound to HER2 receptors on the cell surface and internalized through receptor-mediated endocytosis (Fig. 1*E*). A large proportion of the Affi$_{HER2}$Vacuoles were endocytosed by HER2-overexpressing SKOV3 cells, whereas a relatively low nonspecific uptake was evident in HER2-negative MDA-MB-231 cells. Collectively, these results clearly indicate that the Affi$_{HER2}$Vacuole can be used for cancer-specific targeting and drug delivery. Because of their subnanometer size, the engineered, drug-carrying vacuoles could rapidly extravasate and accumulate in the periphery of tumor tissue, where, after cancer receptor engagement, they could undergo endocytosis before releasing their payload and producing cytotoxic effects. In addition, with the available rapid protocols for vacuole preparation and methods for large-scale fermentation of yeasts, it is possible to obtain high yields of vacuoles in a cost-effective manner (26, 33).

Drug Loading, Quantification, and Release Kinetics. We expected that Dox, a membrane-permeable drug, could be loaded into the membrane and lumen of the Affi$_{HER2}$Vacuole through physical adsorption because the lipid composition of the vacuoles is relatively similar to the lipid composition of mammalian cell membranes (10, 17–19). As shown, the amount of drug loaded in the vacuoles increased by increasing the initial Dox concentration, suggesting that drug loading was mediated by a concentration gradient (Fig. S2*A*). Characterization of the size and shape of the
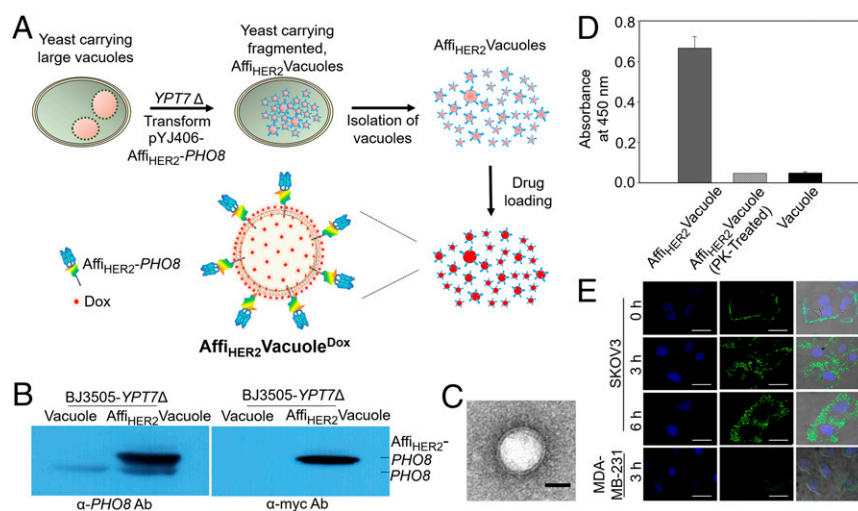

Fig. 1. Generation and characterization of Affi$_{HER2}$Vacuoles. (*A*) Schematic illustration of fragmented vacuole generation and drug loading into anti-HER2 affibody-expressing vacuoles (Affi$_{HER2}$Vacuole^{Dox}). (*B*) Western blot analysis of *PHO8*-affibody and myc-tagged affibody in Affi$_{HER2}$Vacuoles. The analyses confirmed the localization of the affibody in vacuoles as a fusion partner. (*C*) Representative TEM image of the Affi$_{HER2}$Vacuoles. (Scale bar: 50 nm.) (*D*) ELISA results showing the specificity of the Affi$_{HER2}$Vacuoles for HER2 protein. Treatment with PK caused almost a complete loss of HER2p affinity. Data represent the mean ± SD of three replicates. (*E*) Confocal images showing cell binding (0 h) and uptake (3 h and 6 h) of Affi$_{HER2}$Vacuoles in HER2-overexpressing SKOV3 cells and HER2-negative MDA-MB-231 cells. The nuclei were stained with DRAQ5 (blue), and Affi$_{HER2}$Vacuoles were stained with anti-affibody antibody (green). Affi$_{HER2}$Vacuoles exhibited receptor-specific binding and internalization in HER2-overexpressing SKOV3 cells, whereas very low and nonspecific uptake was evident in HER2-negative MDA-MB-231 cells. (Scale bars: 20 μm.)

Gujrati et al.

MEDICAL SCIENCES

Dox-loaded vacuoles (Affi$_{HER2}$Vacuole^{Dox}) by ELS and TEM analyses showed that these vesicles retained an intact circular shape (Fig. S2 B and C), confirming that the drug loading did not affect the physical properties of the Affi$_{HER2}$Vacuole. Next, we investigated drug release from Affi$_{HER2}$Vacuole^{Dox}. As shown, less than 10% of the Dox was released during 24 h of incubation at pH 7.4, whereas drug release was accelerated in an acidic (pH 5.1) environment (Fig. S2D). These results suggest that the vacuole structure becomes destabilized or disrupted in an acidic pH environment, like that in the lysosome of a cell, enabling the rapid release of the payload, but remains intact and relatively stable under physiological conditions, minimizing leaking of the loaded drug into the circulatory system. This drug release profile is crucial for reducing nonspecific cytotoxicity caused by the free drug and for improving the terminal half-life ($t_{1/2}$) of the drug in vivo by preventing its rapid metabolism or excretion.

Cellular Drug Delivery and Cytotoxicity of Affi$_{HER2}$Vacuole^{Dox}. We next investigated the cellular uptake and cytotoxic effects of Affi$_{HER2}$Vacuole^{Dox} in various cancer cell lines. As shown in Fig. 2A, compared with the nontargeting Vacuole^{Dox}, Affi$_{HER2}$Vacuole^{Dox} was largely endocytosed by HER2-overexpressing NIH3T6.7 cells. At 1 h and 12 h, the red fluorescence of Dox was detected largely in the cytoplasm (Fig. S3A), indicating that Dox remained associated with the vacuoles. However, after 12 h, most of the Dox had been released and was readily internalized in the nucleus. Although a clear difference in uptake efficiency was observed between both types of Dox-loaded vacuoles, an almost similar pattern of delayed drug release and nuclear uptake was evident with Affi$_{HER2}$Vacuole^{Dox} and Vacuole^{Dox}. In contrast, due to its intrinsic property, the Free^{Dox} could readily penetrate through the cell membrane and internalize into the nuclei, which was observed within 1 h of treatment. The results clearly show the differences in intracellular kinetics of Free^{Dox} and Dox-loaded vacuoles. Furthermore, compared with HER2-overexpressing SKOV3 and NIH3T6.7 cells, HER2-negative MDA-

MB-231 cells exhibited a very low uptake of Affi$_{HER2}$Vacuole^{Dox} (Fig. S3B). These results show that the receptor-specific binding of Affi$_{HER2}$Vacuole^{Dox} is crucial for cellular uptake, whereas drug release from Affi$_{HER2}$Vacuole^{Dox} takes place presumably due to deformation of the Affi$_{HER2}$Vacuole upon lysosomal acidification. Next, the cytotoxic effect of Affi$_{HER2}$Vacuole^{Dox} was quantitatively evaluated with colorimetric 3-[4,5-dimethylthiazol-2-yl]-2,5 diphenyl tetrazolium bromide assays. In contrast to treatment with PBS, vacuole or Vacuole^{Dox} and treatment with Free^{Dox} or Affi$_{HER2}$Vacuole^{Dox} caused significantly greater cytotoxicity after 96 h of incubation (Fig. 2B), reducing cell viability in both the HER2-overexpressing NIH3T6.7 and SKOV3 cells by 75% and 72%, respectively. The cytotoxicity of Free^{Dox} in HER2-negative MDA-MB-231 cells was significantly higher than the cytotoxicity of Affi$_{HER2}$Vacuole^{Dox}, indicating that the HER2-specific targeting of Affi$_{HER2}$Vacuole^{Dox} is necessary for cell-selective cytotoxicity.

Drug Penetration and Cytotoxicity in Multicellular Cultures. In addition to endocytosis, we monitored the transcytosis or penetration of Affi$_{HER2}$Vacuole^{Dox} with NIH3T6.7 cells cultured in multiple layers on a Transwell filter system (Costar). Cells in the Transwell filter system were treated with Free^{Dox}, nontargeting Vacuole^{Dox}, or Affi$_{HER2}$Vacuole^{Dox}, and penetration was assessed as a function of time by monitoring the fluorescence of the cells cultured below the transwell. Drug uptake and accumulation were increased compared with the controls after incubation with Affi$_{HER2}$Vacuole^{Dox} (Fig. S4), suggesting that, following receptor-mediated endocytosis, Affi$_{HER2}$Vacuole^{Dox} might undergo transcytosis through layers of cells. In contrast, Free^{Dox} could not penetrate the cellular layers due to rapid nuclear entrapment and Vacuole^{Dox} exhibited very low transcytosis because of reduced uptake by cells in the transwell and was largely removed by washing.

We next tested the uptake, penetration, and cytotoxic effects of Affi$_{HER2}$Vacuole^{Dox} in 3D spheroid cultures generated from NIH3T6.7 cells. Nonvascularized cancer cell spheroids are known
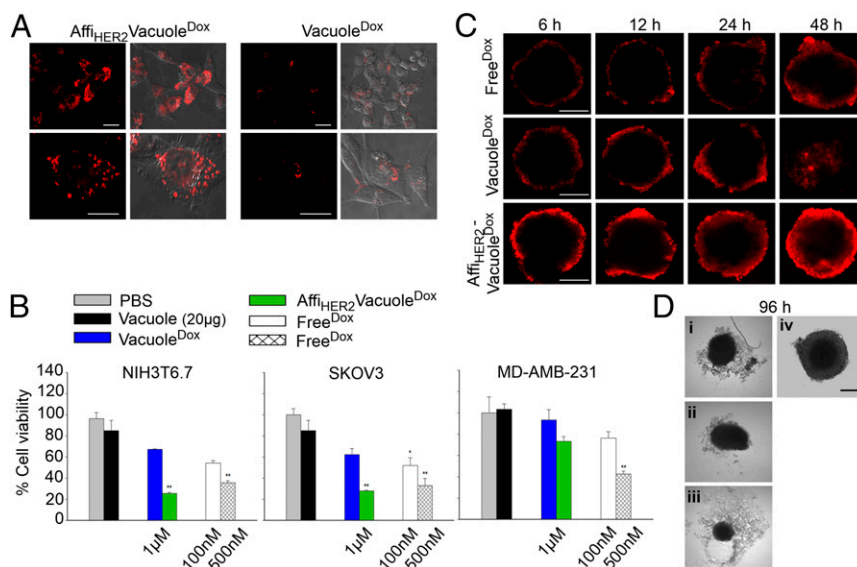

Fig. 2. In vitro drug delivery and cytotoxicity. (A) Confocal images showing in vitro uptake of HER2-targeted Affi$_{HER2}$Vacuole^{Dox} and nontargeting Vacuole^{Dox} by NIH3T6.7 cells. Higher uptake was evident in the Affi$_{HER2}$Vacuole^{Dox}-treated cells. (Scale bars: 20 μm.) (B) In vitro cytotoxic efficacy (analyzed by 3-[4,5-dimethylthiazol-2-yl]-2,5 diphenyl tetrazolium bromide assay) of the Affi$_{HER2}$Vacuole^{Dox} was compared with the in vitro cytotoxic efficacy of various controls in different cell lines (NIH3T6.7, SKOV3, and MD-AMB-231). Cell viability was evaluated after 96 h of incubation with Affi$_{HER2}$Vacuole^{Dox} (Dox: 1 μM) and compared with empty vacuole (20 μg), Vacuole^{Dox} (Dox: 1 μM), and two sets of Free^{Dox} (Dox: 100 nM and 500 nM, respectively). Data represent the mean ± SD of three replicates, expressed relative to the PBS-treated control (**P < 0.01). (C) Confocal images showing the time-dependent uptake and penetration of the Affi$_{HER2}$Vacuole^{Dox} in NIH3T6.7 spheroids. (Scale bar: 200 μm.) (D) Bright-field images of the NIH3T6.7 spheroids after 96 h of treatment with (i) Free^{Dox}, (ii) Vacuole^{Dox}, (iii) Affi$_{HER2}$Vacuole^{Dox}, and (iv) PBS. The cytotoxicity and total volume control were the highest in the Affi$_{HER2}$Vacuole^{Dox}-treated samples compared with the controls. (Scale bar: 200 μm.)

Gujrati et al.

www.manaraa.com

to share several features in common with tumors studied in vivo (34–36). As shown in Fig. 2C, internalization of Free^{Dox} was limited to the outer region of rapidly proliferating cells; such uptake could be attributable to the intrinsic high membrane permeability of the drug. Vacuole^{Dox}, lacking the HER2-binding ability, as well as Free^{Dox} showed a low level of uptake in the spheroids. In contrast, Affi$_{HER2}$Vacuole^{Dox} not only showed a relatively higher uptake in the outer proliferating regions but also penetrated much more deeply into the inner parts of the spheroids, possibly reflecting the advantages of the membrane composition and subnanometer size (mostly below 100 nm) of the vacuoles, which could penetrate more upon saturation of the outer region receptors. The greater penetration and distribution of Affi$_{HER2}$Vacuole^{Dox} in both the transwell and spheroid cultures compared with Free^{Dox} were dependent upon incubation time. Moreover, growth inhibition and volume control of the cancer cell spheroids after 96 h of treatment were much greater with Affi$_{HER2}$Vacuole^{Dox} than with the other controls (Fig. 2D). These results are in accordance with previous in vitro findings, showing that cellular targeting and enhanced penetration improved the efficacy of Dox (35). Taken together, these results show that Affi$_{HER2}$Vacuole^{Dox} can selectively deliver a drug payload to targeted cancer cells and exert cytotoxic effects. Importantly, Affi$_{HER2}$Vacuole alone is not cytotoxic in cells; therefore, the targeted Affi$_{HER2}$Vacuole^{Dox} system could be used to safely treat cancers in vivo.

In Vivo Cancer Targeting, Biodistribution, and Antitumor Efficacy. Researchers have developed a variety of nanocarriers to improve the therapeutic index of drugs, mainly by increasing their efficacy and reducing their toxic side effects. However, curtailing vector-associated toxicity is technically challenging. Therefore, biomaterials that are biocompatible, bioresponsive, and biodegradable could be advantageous over synthetic vectors and continue to be actively developed (8, 9). To investigate the tumor targeting and therapeutic efficacy of Affi$_{HER2}$Vacuole^{Dox} in vivo, we used a HER2-overexpressing NIH3T6.7 cell-based mouse xenograft model (37). Mice bearing NIH3T6.7 xenografts were systemically injected with Affi$_{HER2}$Vacuole^{Dox}, Vacuole^{Dox}, or Free^{Dox} via the tail vein, and tumor tissue sections were analyzed for cellular drug distribution at fixed time points (6 h and 12 h) by monitoring the red fluorescence of the accumulated Dox. Images obtained from the various tissue sections (from the top to the center) of each tumor showed strong Dox fluorescence in the Affi$_{HER2}$Vacuole^{Dox}-injected animals compared with the control animals (Fig. 3A and Fig. S5A). The results show a greater accumulation and penetration of the Affi$_{HER2}$Vacuole^{Dox} compared with the controls. Although Vacuole^{Dox} showed a relatively low cellular uptake due to passive targeting, its enhanced distribution, like the enhanced distribution of the Affi$_{HER2}$Vacuole^{Dox}, ensures the effectiveness of biological carriers in penetrating tissue deeply. By comparison, the least accumulation was observed with Free^{Dox}, indicating that passive targeting prevents effective accumulation in tumors and that the drug is cleared through the circulation. We extended this analysis by assessing the biodistribution of Affi$_{HER2}$Vacuole^{Dox} compared with the biodistribution of nontargeting Vacuole^{Dox} and Free^{Dox} in NIH3T6.7 xenograft mice with each i.v.-administered formulation at a Dox dose of 1 mg/kg. Tumors and vital organs were collected 6 h postinjection to quantify the drug. As shown in Fig. 3B, animals injected
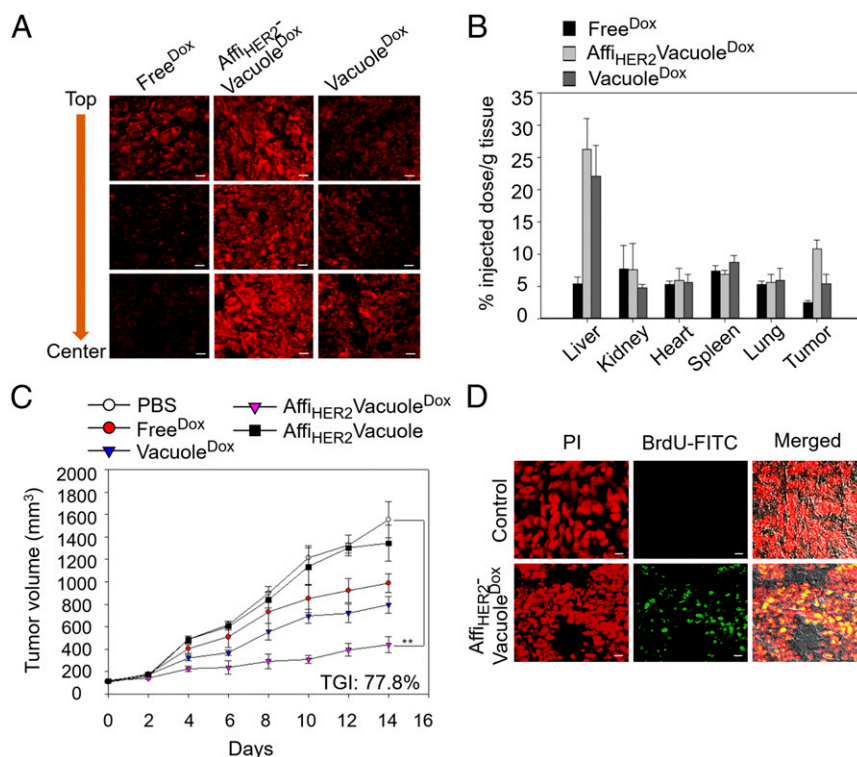

Fig. 3. In vivo tumor targeting, biodistribution, and antitumor effects of Affi$_{HER2}$Vacuole^{Dox} in NIH3T6.7 xenograft mice. (A) Confocal images of tumor sections show the drug distribution in cancer cells after 6 h of treatment with Affi$_{HER2}$Vacuole^{Dox} (1 mg/kg) compared with the controls. (Scale bars: 10 μm.) (B) Tumor-specific distribution of Affi$_{HER2}$Vacuole^{Dox} (1 mg/kg) analyzed 6 h after i.v. administration in NIH3T6.7 xenograft mice. Values are reported as the mean ± SD of triplicate samples. (C) Tumor growth was monitored throughout the course of the treatment (Dox at a dose of 1 mg/kg administered every other day) in each treatment group. The percentage of tumor growth inhibition (TGI) caused by Affi$_{HER2}$Vacuole^{Dox} was evaluated on the final day of treatment by comparison with PBS-treated controls; each value represents the mean ± SD (**$P < 0.01$ vs. control; $n = 5$ mice per group). (D) Apoptosis was determined by TUNEL assay measured as BrdU-FITC–positive cells (green) in tumor tissue sections from animals treated with Affi$_{HER2}$Vacuole^{Dox} compared with PBS controls. (Scale bars: 10 μm.) PI, propidium iodide.

Gujrati et al.

MEDICAL SCIENCES

www.manaraa.com

with $Affi_{HER2}Vacuole^{Dox}$ or $Vacuole^{Dox}$ showed a relatively greater tumor accumulation of Dox compared with animals injected with $Free^{Dox}$, suggesting the extended $t_{1/2}$ of Dox-carrying vacuoles resulted in enhanced distribution to tumors. Furthermore, a comparison of targeted and nontargeted delivery showed a greater tumor-specific retention and accumulation of the HER2-targeted $Affi_{HER2}Vacuole^{Dox}$ (~11% injected dose per gram of tissue), suggesting that the HER2-specific affibody is responsible for the improved tumor-specific accumulation of the drug. To evaluate the behavior of $Affi_{HER2}Vacuole^{Dox}$ and validate if the vacuole-based formulation could prolong the systemic circulation of Dox, the pharmacokinetic parameters were evaluated in tumor-free mice. The $Affi_{HER2}Vacuole^{Dox}$ and $Free^{Dox}$ were administered i.v., and the plasma drug concentrations were measured as a function of time. The $Affi_{HER2}Vacuole^{Dox}$ showed the highest level of Dox retention in the circulation compared with $Free^{Dox}$ (Fig. S5B). The pharmacokinetic parameters obtained after fitting the data in a noncompartmental pharmacokinetic model are also given (Fig. S5B). The terminal $t_{1/2}$ and area under the curve (AUC) of $Affi_{HER2}Vacuole^{Dox}$ were 6.16-fold and 15.37-fold higher, respectively, than the terminal $t_{1/2}$ and AUC of $Free^{Dox}$. Taken together, these results suggest that the HER2-targeted $Affi_{HER2}Vacuole^{Dox}$ performed well as a targeted drug delivery platform. Importantly, $Affi_{HER2}Vacuole^{Dox}$ was able to circulate for a significantly longer period. An extended $t_{1/2}$, which ensures enhanced extravasation and receptor-specific endocytosis, is an essential parameter that achieves effective delivery of the cargo and long-term accumulation of the drug at the target tumor site.

We next compared the antitumor efficacy of $Affi_{HER2}Vacuole^{Dox}$ with the antitumor efficacy of the nontargeting $Vacuole^{Dox}$ and $Free^{Dox}$ in NIH3T6.7 xenografts. After the tumors had become established, mice were divided into five groups: (i) vehicle control (PBS-treated), (ii) empty $Affi_{HER2}Vacuole$, (iii) $Free^{Dox}$ (1 mg/kg), (iv) nontargeting $Vacuole^{Dox}$ (1 mg/kg), and (v) HER2-targeted $Affi_{HER2}Vacuole^{Dox}$ (1 mg/kg). Each regimen was administered i.v. every other day for a total of eight injections. Tumor growth rates and animal body weights were recorded during the course of each treatment. Tumor growth was significantly delayed in mice injected with $Affi_{HER2}Vacuole^{Dox}$ compared with mice injected with PBS, empty $Affi_{HER2}Vacuole$, nontargeting $Vacuole^{Dox}$, or $Free^{Dox}$ (Fig. 3C and Fig. S6A). The percentage of tumor growth inhibition on the last day of the $Affi_{HER2}Vacuole^{Dox}$ treatment was 77.8%. Next, the harvested tumors were weighed and analyzed to assess the mechanism of cell killing. Consistent with the observed regression of tumor growth, the average weight of the excised tumors was significantly less in the $Affi_{HER2}Vacuole^{Dox}$-treated group than in the control groups (Fig. S6B). Throughout the treatment, the animals in all of the groups appeared normal, showing no overt signs of toxicity and a consistent body weight (Fig. S6C). Finally, the apoptosis of cells in the tumor tissue was assessed with TUNEL staining. This assay revealed abundant BrdU-FITC–positive apoptotic cells in the tumors excised from the mice treated with $Affi_{HER2}Vacuole^{Dox}$ (Fig. 3D and Fig. S6D). Consistent with the drug distribution results, tumors from mice treated with $Free^{Dox}$ or nontargeting $Vacuole^{Dox}$ showed minimal apoptosis; no signs of apoptosis were detected in mice treated with PBS or empty $Affi_{HER2}Vacuole$. Moreover, the HER2-specific targeting of $Affi_{HER2}Vacuole^{Dox}$ enabled a preferential concentration of the drug in the tumor tissue through the enhanced permeability and retention effect, as well as the promotion of the subsequent receptor-mediated endocytosis and intratumoral distribution. Collectively, these results indicate that nanocarrier-based drug delivery and active targeting substantially enhance therapeutic efficacy and increase the therapeutic index of the drug.

Cytotoxicity and Immune Responses. To test the cytotoxic effects of the vacuoles in vitro, we treated human umbilical vein endothelial cells (HUVECs) with either wild type (WT) or $Affi_{HER2}$-modified vacuoles for 24 h, and evaluated the apoptotic effects by immunostaining. Compared with the vehicle control (methanol)-treated cells, vacuole-treated cells appeared normal; no signs of cytotoxicity were evident, and overall cell viability remained high (Fig. S7A).

Next, we evaluated vacuole-induced immune responses both in vitro and in vivo. For the in vitro analyses, we stimulated murine macrophage-like RAW 264.7 cells with either form of the vacuole; LPS was used as a positive control. The TNF-α levels in the vacuole-treated cells were indistinguishable from the TNF-α levels in the PBS-treated cells (Fig. S7B), whereas LPS caused a significant and substantial cytokine response. These results suggest that the vacuoles used herein are very weakly immunogenic and could be well tolerated upon systemic administration. To confirm the in vivo safety of the vacuoles, we investigated whether repeated systemic injection of vacuoles (WT or $Affibody_{HER2}$-modified) overstimulated the immune system. Immune responses were recorded in C57BL/6 mice after systemic administration of 100 or 200 µg of vacuoles for 4 consecutive days by measuring the serum levels of TNF-α, IL-6, and IFN-γ with ELISA. Cytokine levels were evaluated at two time points, 2 h and 24 h, to monitor early and delayed immune responses. Both forms of vacuoles slightly increased the serum levels of TNF-α and IL-6 at the early (2-h) time point but had no effect on IFN-γ levels under any condition (Fig. 4). Importantly, however, cytokine levels returned to baseline by 24 h in all treatment groups. Moreover, there was no significant difference in immune stimulation at the two different concentrations of vacuoles, and neither treatment resulted in body weight loss or lethality. These results suggest that the vacuoles are nontoxic and well tolerated upon systemic administration. Therefore, the vacuoles themselves do not likely contribute to the antitumor effects by overstimulating immune pathways and, as such, are safe for in vivo systemic administration. Although these preliminary results in mice are encouraging, further blood chemistry and safety profile analyses in higher animals will be required.
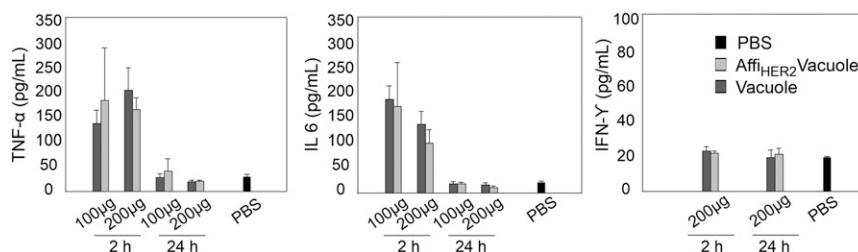

Fig. 4. Investigation of immune responses upon treatment with $Affi_{HER2}$Vacuoles in C57BL/6 mice. The serum levels of cytokines TNF-α, IL-6, and IFN-γ were quantified by ELISA. Analyses were performed at early (2 h) and late (24 h) time points after treatment with PBS or vacuoles (WT or $Affi_{HER2}$-modified: 100 µg and 200 µg each) for 4 consecutive days. Each value represents the mean ± SD (n = 5 mice per group) and was analyzed as described in *SI Materials and Methods*, *Serum Cytokine Analysis*.

Conclusion

In conclusion, the proposed approach suggests a platform technology for generating cancer-specific, tissue-penetrating, safe, and scalable biological nanoparticles from a nonhazardous yeast strain as a potential targeted cancer therapy. The developed nanocarriers can be generated on a large scale in a cost-effective manner by optimizing the fermentation and purification methods. The results showed significant tumor growth inhibition due to active drug delivery, enhanced biodistribution within tumors, and minimal toxic side effects using $Affi_{HER2}Vacuole^{Dox}$, suggesting that bioengineered vacuoles have potential for use as drug delivery carriers in treating cancers. In the future, we plan to investigate the possibility of loading diverse therapeutic agents, including toxins, within vacuoles and testing their fate, both in vitro and in vivo.

Materials and Methods

Detailed methods on the following subjects are available in *SI Materials and Methods*: yeast strains, plasmid construction, and vacuole isolation; cell culture and spheroid preparation; characterization of the vacuoles; cell binding and uptake assay; characterization of drug-loaded vacuoles; in vitro drug delivery and cytotoxicity; xenograft model, in vivo targeting, biodistribution and pharmacokinetic analysis; in vivo antitumor effects in NIH3T6.7 xenografts; HUVEC cytotoxicity study; RAW 264.7 cell stimulation assay; serum cytokine analysis; and statistical analyses. All animal experiments were done according to established guidelines and with the approval of the KAIST-Institutional Animal Care Committee (KA2013-25).

1. Davis ME, Chen ZG, Shin DM (2008) Nanoparticle therapeutics: An emerging treatment modality for cancer. *Nat Rev Drug Discov* 7(9):771–782.
2. Chauhan VP, Jain RK (2013) Strategies for advancing cancer nanomedicine. *Nat Mater* 12(11):958–962.
3. Shi J, Votruba AR, Farokhzad OC, Langer R (2010) Nanotechnology in drug delivery and tissue engineering: From discovery to applications. *Nano Lett* 10(9):3223–3230.
4. Chow EKH, Ho D (2013) Cancer nanomedicine: From drug delivery to imaging. *Sci Transl Med* 5(216):216rv4.
5. Adair JH, Parette MP, Altinoğlu EI, Kester M (2010) Nanoparticulate alternatives for drug delivery. *ACS Nano* 4(9):4967–4970.
6. Peer D, et al. (2007) Nanocarriers as an emerging platform for cancer therapy. *Nat Nanotechnol* 2(12):751–760.
7. Petros RA, DeSimone JM (2010) Strategies in the design of nanoparticles for therapeutic applications. *Nat Rev Drug Discov* 9(8):615–627.
8. Desai N (2012) Challenges in development of nanoparticle-based therapeutics. *AAPS J* 14(2):282–295.
9. Yoo JW, Irvine DJ, Discher DE, Mitragotri S (2011) Bio-inspired, bioengineered and biomimetic drug delivery carriers. *Nat Rev Drug Discov* 10(7):521–535.
10. MacDiarmid JA, et al. (2007) Bacterially derived 400 nm particles for encapsulation and cancer cell targeting of chemotherapeutics. *Cancer Cell* 11(5):431–445.
11. Alvarez-Erviti L, et al. (2011) Delivery of siRNA to the mouse brain by systemic injection of targeted exosomes. *Nat Biotechnol* 29(4):341–345.
12. Gujrati V, et al. (2014) Bioengineered bacterial outer membrane vesicles as cell-specific drug-delivery vehicles for cancer therapy. *ACS Nano* 8(2):1525–1537.
13. MacDiarmid JA, et al. (2009) Sequential treatment of drug-resistant tumors with targeted minicells containing siRNA or a cytotoxic drug. *Nat Biotechnol* 27(7):643–647.
14. Jang SC, et al. (2013) Bioinspired exosome-mimetic nanovesicles for targeted delivery of chemotherapeutics to malignant tumors. *ACS Nano* 7(9):7698–7710.
15. Nevoigt E (2008) Progress in metabolic engineering of Saccharomyces cerevisiae. *Microbiol Mol Biol Rev* 72(3):379–412.
16. A A (1992) Yeast genome project:300,000 and counting. *Science* 256(5056):462.
17. Armstrong J (2010) Yeast vacuoles: More than a model lysosome. *Trends Cell Biol* 20(10):580–585.
18. Klionsky DJ, Herman PK, Emr SD (1990) The fungal vacuole: Composition, function, and biogenesis. *Microbiol Rev* 54(3):266–292.
19. Weisman LS (2003) Yeast vacuole inheritance and dynamics. *Annu Rev Genet* 37:435–460.
20. Weisman LS (2006) Organelles on the move: Insights from yeast vacuole inheritance. *Nat Rev Mol Cell Biol* 7(4):243–252.
21. Orlova A, et al. (2006) Tumor imaging using a picomolar affinity HER2 binding affibody molecule. *Cancer Res* 66(8):4339–4348.
22. Qvarnström OF, Simonsson M, Carlsson J, Tran TA (2011) Effects of affinity on binding of HER2-targeting Affibody molecules: Model experiments in breast cancer spheroids. *Int J Oncol* 39(2):353–359.
23. Li SC, Kane PM (2009) The yeast lysosome-like vacuole: Endpoint and crossroads. *Biochim Biophys Acta* 1793(4):650–663.
24. Ostrowicz CW, Meiringer CTA, Ungermann C (2008) Yeast vacuole fusion: A model system for eukaryotic endomembrane dynamics. *Autophagy* 4(1):5–19.
25. Wickner W (2010) Membrane fusion: Five lipids, four SNAREs, three chaperones, two nucleotides, and a Rab, all dancing in a ring on yeast vacuoles. *Annu Rev Cell Dev Biol* 26:115–136.
26. Wickner W (2002) Yeast vacuoles and membrane fusion pathways. *EMBO J* 21(6):1241–1247.
27. Haas A, Scheglmann D, Lazar T, Gallwitz D, Wickner W (1995) The GTPase Ypt7p of Saccharomyces cerevisiae is required on both partner vacuoles for the homotypic fusion step of vacuole inheritance. *EMBO J* 14(21):5258–5270.
28. Jun Y, Wickner W (2007) Assays of vacuole fusion resolve the stages of docking, lipid mixing, and content mixing. *Proc Natl Acad Sci USA* 104(32):13010–13015.
29. Coonrod EM, et al. (2013) Homotypic vacuole fusion in yeast requires organelle acidification and not the V-ATPase membrane domain. *Dev Cell* 27(4):462–468.
30. Zieger M, Mayer A (2012) Yeast vacuoles fragment in an asymmetrical two-phase process with distinct protein requirements. *Mol Biol Cell* 23(17):3438–3449.
31. Segev N (2001) Ypt and Rab GTPases: Insight into functions through novel interactions. *Curr Opin Cell Biol* 13(4):500–511.
32. Hickey CM, Stroupe C, Wickner W (2009) The major role of the Rab Ypt7p in vacuole fusion is supporting HOPS membrane association. *J Biol Chem* 284(24):16118–16125.
33. Wiederhold E, et al. (2009) The yeast vacuolar membrane proteome. *Mol Cell Proteomics* 8(2):380–392.
34. Kunz-Schughart LA (1999) Multicellular tumor spheroids: Intermediates between monolayer culture and in vivo tumor. *Cell Biol Int* 23(3):157–161.
35. Perche F, Patel NR, Torchilin VP (2012) Accumulation and toxicity of antibody-targeted doxorubicin-loaded PEG-PE micelles in ovarian cancer cell spheroid model. *J Control Release* 164(1):95–102.
36. Hirschhaeuser F, et al. (2010) Multicellular tumor spheroids: An underestimated tool is catching up again. *J Biotechnol* 148(1):3–15.
37. Lee JH, et al. (2007) Artificially engineered magnetic nanoparticles for ultra-sensitive molecular imaging. *Nat Med* 13(1):95–99.
38. Haas A, Wickner W (1996) Homotypic vacuole fusion requires Sec17p (yeast alpha-SNAP) and Sec18p (yeast NSF). *EMBO J* 15(13):3296–3305.
39. Ko YJ, Lee M, Kang K, Song WK, Jun Y (2014) In vitro assay using engineered yeast vacuoles for neuronal SNARE-mediated membrane fusion. *Proc Natl Acad Sci USA* 111(21):7677–7682.
40. Friedrich J, Seidel C, Ebner R, Kunz-Schughart LA (2009) Spheroid-based drug screen: Considerations and practical approach. *Nat Protoc* 4(3):309–324.
41. Yu MK, et al. (2008) Drug-loaded superparamagnetic iron oxide nanoparticles for combined cancer imaging and therapy in vivo. *Angew Chem Int Ed Engl* 47(29):5362–5365.
42. Bagalkot V, Farokhzad OC, Langer R, Jon S (2006) An aptamer-doxorubicin physical conjugate as a novel targeted drug-delivery platform. *Angew Chem Int Ed Engl* 45(48):8149–8152.
43. Tagami T, Ernsting MJ, Li SD (2011) Efficient tumor regression by a single and low dose treatment with a novel and enhanced formulation of thermosensitive liposomal doxorubicin. *J Control Release* 152(2):303–309.
44. Letsch M, Schally AV, Busto R, Bajo AM, Varga JL (2003) Growth hormone-releasing hormone (GHRH) antagonists inhibit the proliferation of androgen-dependent and -independent prostate cancers. *Proc Natl Acad Sci USA* 100(3):1250–1255.
45. Hajjar AM, Ernst RK, Tsai JH, Wilson CB, Miller SI (2002) Human Toll-like receptor 4 recognizes host-specific LPS modifications. *Nat Immunol* 3(4):354–359.

Gujrati et al.

MEDICAL SCIENCES

www.manaraa.com